Combining doxorubicin-nanobubbles and shockwaves for Anaplastic thyroid cancer treatment: Preclinical study in a xenograft mouse model

Combining doxorubicin-nanobubbles and shockwaves for anaplastic thyroid cancer treatment: preclinical study in a xenograft mouse model

Francesca Marano[1], Roberto Frairia[1], Letizia Rinella[1], Monica Argenziano[2], Benedetta Bussolati[3], Cristina Grange[1], Raffaella Mastrocola[4], Isabella Castellano[1], Laura Berta[5], Roberta Cavalli[2], Maria Graziella Catalano[1]

[1]Department of Medical Sciences, University of Turin, Turin, Italy;

[2]Department of Drug Science and Technology, University of Turin, Turin, Italy;

[3]Department of Molecular Biotechnology and Health Sciences, University of Turin, Turin, Italy;

[4]Department of Clinical and Biological Sciences, University of Turin, Turin, Italy;

[5]Med & Sport 2000 Srl, Turin, Italy.

Corresponding Author: Maria Graziella Catalano, Department of Medical Sciences, University of Turin, Via Genova 3, 10126 Turin, Italy; tel. +39-0116705360; fax. +39-0116705366; mail: mariagraziella.catalano@unito.it

Short title: Doxorubicin NBs and ESWs for ATC treatment.

Keywords: Extracorporeal shock waves; nanobubbles; doxorubicin; anaplastic thyroid cancer; drug delivery

Word Count: 4661

Abstract

Anaplastic thyroid cancer is one of the most lethal diseases and a curative therapy does not exist. Doxorubicin, the only drug approved for anaplastic thyroid cancer treatment, has a very low response rate and causes numerous side effects among which cardiotoxicity is the most prominent. Thus, doxorubicin delivery to the tumor site could be an import goal aimed to improve drug efficacy and to reduce its systemic side effects. We recently reported that, in human anaplastic thyroid cancer cell lines, combining doxorubicin-loaded nanobubbles with extracorporeal shock waves, acoustic waves used in lithotripsy and orthopedics without side effects, increased the intracellular drug content and *in vitro* cytotoxicity. In the present study we tested the efficacy of this treatment on a human anaplastic thyroid cancer xenograft mouse model. After 21 days, the combined treatment determined the greatest drug accumulation in tumors with consequent reduction of tumor volume and weight, and an extension of the tumor doubling time. Mechanistically, the treatment induced tumor apoptosis and decreased cell proliferation. Finally, whereas doxorubicin caused the increase of fibrosis markers and oxidative stress in animal hearts, loading doxorubicin into nanobubbles avoided these effects preventing heart damage.

The improvement of doxorubicin anti-tumor effects together with the prevention of heart damage suggests that the combination of doxorubicin-loaded nanobubbles with extracorporeal shock waves might be a promising drug delivery system for anaplastic thyroid cancer treatment.

Introduction

Anaplastic thyroid cancer (ATC) is one of the most lethal cancers, being its median survival of only 5 months and 1-year survival less than 20% (Smallridge and Copland 2010). To date a standard therapy for ATC does not exist. The American Thyroid Association (Smallridge *et al.* 2012) and the National Comprehensive Cancer Network guidelines® (Haddad *et al.* 2015) suggest a multimodal approach including extensive resection followed by adjuvant chemo-radiotherapy. Nevertheless, the management of ATC remains a challenge and ATC is still an incurable disease. Doxorubicin is the only cytotoxic drug approved for the treatment in monotherapy of ATC (Haddad *et al.* 2015). Unfortunately, it has a response rate below 22% (Giuffrida *et al.* 2000) and, if not specifically targeted to the tumor cells, it causes severe side effects, among which cardiotoxicity is the most prominent. Notably, the severity of cardiac side effects and their occurrence are dose dependent (Minotti *et al.* 2004, Chatterjee *at al.* 2010, Zhang *et al.* 2012). Therefore, there is an increasing attention towards the development of new doxorubicin formulations to specifically deliver the drug to the tumor site increasing its anti-tumor efficacy and reducing its toxicity. To this aim, many formulations of doxorubicin-loaded nanoparticles have been developed (Wohlfart *et al.* 2011, Barenholz 2012, Golla *et al.* 2013, Yu *et al.* 2014, Razavi-Azarkhiavi *et al.* 2016). In general, nanoparticles can carry loaded drugs to the tumor site through the blood stream taking advantage of the enhanced permeability and retention effect, due to the defective vascular architecture of the tumor (Fang *et al* 2011). However, the universal role and advantages of enhanced permeability and retention effect in cancer therapy are still debated. In fact, vessel leakage, the absence of a functional lymphatic system and increased extracellular matrix frictional resistance, increase tumor interstitial fluid pressure and ultimately provoke disruption in blood flow directions, limiting drug delivery (Azzi *et al.* 2013, Carmeliet and Jain 2011). To overcome this problem, a better drug delivery to cancer tissues can be obtained by combining physical triggers (e.g. ultrasounds, US) to gas-cored micro and nanobubbles (NBs) (Gao *et al.* 2008, Collis *at al.* 2010, Cavalli *et al.* 2012,

Cavalli *et al.* 2016). Indeed, US causes bubble cavitation resulting in cell sonoporation and allowing the extravasation of molecules (Collis *et al* 2010). Extracorporeal Shock Waves (ESWs) are short-duration focused acoustic waves widely used in urology for lithotripsy (Rassweiler *et al.* 2011) and, more recently, in several musculoskeletal diseases (Wang 2012). ESWs can be focused with high precision in depth and they determine permeabilization of plasma membranes (Lauer *et al.* 1997, Kodama *et al.* 2002, Frairia *et al.* 2003, Catalano *et al.* 2007). As a consequence of ESW-induced cell permeability, ESWs increase the cytotoxic effects of different anti-cancer drugs (Frairia *et al.* 2003, Palmero *et al.* 2006, Catalano *et al.* 2007, Canaparo et al. 2008). All these features make ESWs an ideal tool to be used in combination with drug-loaded NBs. In line with this hypothesis, we recently demonstrated that new perfluoropentane-cored glycol chitosan NBs loaded with doxorubicin released the drug in response to ESW treatment in stabilized human ATC cell lines, resulting in increased intracellular drug content and enhanced doxorubicin cytotoxicity (Marano *et al.* 2016). Aim of the present study was to evaluate the *in vivo* efficacy of combining these doxorubicin-loaded NBs and ESWs in an ATC xenograft model with the final intent to improve doxorubicin anti-tumor effects and to reduce doxorubicin-induced cardiotoxicity.

Materials and Methods

Nanobubble formulations. Empty and doxorubicin-loaded perfluoropentane-cored glycol chitosan NBs were prepared by purposely tuning the method reported elsewhere (Marano *et al.* 2016) reaching a final amount of incorporated drug up to 150 μg/ml. Physico-chemical characterization, loading capacity and encapsulation efficiency of nanobubbles, were determined as described in previous study (Marano *et al.* 2016).

Cell line. Stabilized ATC cell line CAL-62 was purchased from Deutsche Sammlung von Mikroorganismen and Zellkulturen (Braunschweig, Germany), which certifies the origin and identity of the cells. Cells were routinely maintained in 75 cm^2 flasks at 37°C, in 5% CO_2 and 95% humidity, with 100 IU/ml penicillin and 100 μg/ml streptomycin (Gibco, Life Technologies Corp., Grand Island, NY, USA) added in DMEM-F12 (Invitrogen, Groningen, The Netherlands) supplemented with 10% FCS (Euroclone, Wetherby, West York, UK). CAL-62 cells are included in the list of the authenticated unique thyroid cancer cell lines (Schweppe *et al.* 2008).

Xenograft model. The study was conducted on *Mus musculus* in accordance with the national guidelines for the care and use of research animals, and was approved by the Ethics Committee of the University of Turin and by the Italian Board of Health with authorization n.492/2015-PR. Suspension of 5 x 10^5 CAL-62 cells in Matrigel (1:1) (Corning, New York, NY, USA) was injected under the skin in the two flanks of 7-week-old female NOD Scid Gamma (NSG) mice (Molecular Biotechnology Center, Turin, Italy). When tumors reached a minimum volume of 100 mm^3, animals were randomly assigned to different treatment groups.

To determine the time needed to deliver NBs to the tumors, 0.75 mg/kg doxorubicin-loaded NBs were intravenously (i.v.) injected in the animal tail vein. After 0.5, 1.5, 5 and 24 hours, mice (n=5 per group) were sacrificed and doxorubicin was quantified in tumors by High Performance Liquid Chromatography (HPLC) as described below (doxorubicin quantification paragraph).

For all the other *in vivo* experiments, 100 μl 0.9% (v/v) saline solution (CTRL; n=5), or 0.75 mg/kg doxorubicin solution (DOXO; n=5), or 0.75 mg/kg doxorubicin-loaded glycol chitosan NBs (NBs-DOXO; n=5) were i.v. injected into the tail vein.

At the selected time, each mouse was anesthetized by intramuscular injection with 80 mg/kg tiletamine/zolazepam (Zoletil® 100, Virbac, France) and 16 mg/kg xylazine (Rompun, Bayer SpA, Germany) and treated with ESWs (0.59 mJ/mm^2, 500 pulses) on one of the two tumors. A piezoelectric shock wave generator (Piezoson 100, Richard Wolf, Knittlingen, Germany), provided by Med & Sport 2000 S.r.l., Torino, Italy, was used for the study. This device generates focused underwater shock waves at various frequencies (1-4 pulses/s) and intensities (0.05-1.48 mJ/mm^2). Shock wave intensity is the energy at the focal point, defined as energy flux density (EFD) per impulse recorded as joules per area (mJ/mm^2). The focus volume is defined as the zone where 50% of the maximum energy is delivered; with regard to the Piezoson 100, the focus zone has a length of 10 mm in the direction of the axis of the shock wave propagation and a diameter of 2.5 mm perpendicular to this axis. For treating mice, the hair over the tumor was shaved and ultrasound gel applied to the naked skin. The transducer was placed in close contact with the tumor. The position and the angle of the mouse were adjusted to locate the tumor at the focal spot and, thus, allow the focused wave to propagate throughout the cancer.

Treatments were repeated once a week for a total duration of 21 days. Tumor volume was assessed every seven days. Tumors were measured with calipers and volumes were calculated with the formula a^2 x b x 0.5, where a is the shortest diameter and b is the diameter perpendicular to a. Doubling time of tumor volume was calculated according the following formula: $T \times \log_2/(\log V_f - \log V_i)$; where V_f is the final tumor volume, V_i is the initial tumor volume, and T is the time interval (days) between V_f and V_i (Guo *et al.* 2009).

At sacrifice, tumors and hearts were collected. Tumors were weighted and photographed by digital camera. Pieces of tumors and hearts were either fixed in 10% buffered formalin, or frozen, or put in All Protect Tissue Reagent (Life Science, Italy).

Doxorubicin quantification. Tissue extracts from frozen tumors and hearts were prepared by adding one volume of methanol followed by two volumes of 1 M Tris buffer pH 8.5. The mixtures were homogenized using Polytron® (Kinematica GMBH, Eschbach, Germany) and the tissue homogenates kept on ice for 15 min before adding seven volumes of acetonitrile. The mixtures were vortexed and allowed to stand at room temperature for 15 min before removing the precipitated proteins by centrifugation at 3000 *x g* for 5 min. After centrifugation, clear supernatants were assessed for doxorubicin content by HPLC. HPLC system consisted of a pump (LC-9A PUMP C, Shimadzu, Japan) equipped with a fluorescence detector (Chrompack, Japan) and analyses were performed using an Agilent TC C18 column (250 mm × 4.6 mm, 5 μm). To calculate the drug concentration a linear calibration curve was set up with a concentration range of 0.025−2.5 μg/ml with a regression coefficient of 0.999.

Tunel assay. Apoptosis was evaluated by TUNEL (terminal deoxynucleotidyl transferase-mediated dUTP nick end labeling) assay (ApopTag Plus, Millipore, Billerica, MA, USA). Briefly, paraffin embedded slices of tumors were deparaffined and TUNEL assay was performed following the manufacturer's instruction. Positive cells were stained by brown precipitated of oxidized 3,3'-diaminobenzidine (DAB) (Dako, Agilent Technologies, Santa Clara, CA, USA). Slides were observed under optical microscope Olympus AX70 provis (Olympus Optical CO., Hamburg, Germany). To count positive cells, pictures were acquired by digital camera suite Leica Application Suite X 2.0.0.14332 (Leica Microsystems, Wetzlar, Germany). After excluding areas of necrosis, the number of apoptotic cells per field was counted in 10 randomly chosen sections using x200 final magnification.

Proliferating Cell Nuclear Antigen (PCNA). Tumor paraffin sections were deparaffined and probed using an anti-PCNA antibody (1:300 dilution in PBS 0.1% BSA; Santa Cruz Biotechnology, CA, USA). Secondary antibody was a goat anti-mouse Horseradish Peroxidase (HPR)-conjugated antibody (1:300 dilution in PBS 0.1% BSA; Thermo Fisher Scientific, Waltham, Massachusetts, USA). DAB (Dako, Agilent Technologies, Santa Clara, CA, USA) was used as substrate of HPR conjugated to secondary antibody. To count PCNA positive cells, pictures were acquired by digital camera suite Leica Application Suite X 2.0.0.14332 (Leica Microsystems, Wetzlar, Germany). The ten fields with the highest density of positive nuclei were captured at x200 final magnification and positive *vs* total cells were counted using ImageJ software. Only nuclei with a strongly positive label were counted.

Hematoxylin and Eosin stain. Heart paraffin sections were deparaffined and stained with hematoxylin and eosin. Scansions of the entire slides were captured by Aperio ScanScope slide scanner (Leica Microsystems, Wetzlar, Germany).

Masson's trichrome stain. Collagen fibers in hearts were detected by Masson's trichrome stain kit (Bio-Optica Milano S.p.a., Milan, Italy). Briefly, paraffin embedded slices of hearts were deparaffined and trichrome stain was performed following the manufacturer's instruction. Collagen fibers were stained by Aniline Blue Solution included in the kit. Slides were observed under optical microscope Olympus AX70 provis (Olympus Optical CO., Hamburg, Germany). Pictures were acquired by digital camera suite Leica Application Suite X 2.0.0.14332 (Leica Microsystems, Wetzlar, Germany). The percentage of blue area *vs* total area was counted in ten randomly chosen fields at x200 final magnification using ImageJ software.

Gene expression. Total RNA was extracted from heart pieces, homogenizing tissues by Polytron (Kinematica GMBH, Eschbach, Germany) in TRIzol Reagent (Invitrogen Ltd, Paisley, UK). DNase I was added to remove remaining genomic DNA. 1 μg total RNA was reverse-transcribed with iScript cDNA Synthesis Kit (BioRad Laboratories, Inc.), following the manufacturer's protocol.

Primers (Table 2) were designed using Beacon Designer 5.0 software according to parameters outlined in the BioRad iCycler Manual. Specificity of primers was confirmed by BLAST analysis. Real-time PCR was performed using a BioRad iQ iCycler Detection System (BioRad Laboratories, Inc.) with SYBR green fluorophore. Reactions were performed in a total volume of 25 μl including 12.5 μl IQ SYBR Green Supermix (BioRad Laboratories, Inc.), 1 μl of each primer at 10 μM concentration, and 5 μl of the previously reverse-transcribed cDNA template. Protocol for primer set up was optimized using seven serial 5X dilutions of template cDNA obtained from cells in basal conditions. The protocol used is as follows: denaturation (95°C for 5 min), amplification repeated 40 times (95°C for 15 sec, 60°C for 30 sec). A melting curve analysis was performed following every run to ensure a single amplified product for every reaction. All reactions were carried out at least in triplicate for each sample. Results were normalized using the geometric mean for three different housekeeping genes (ribosomal protein L13A, ribosomal protein large P0, and glyceraldehyde-3-phosphate dehydrogenase) and expressed as relative expression fold *vs* untreated controls.

Protein extraction. Total proteins were extracted from heart tissue homogenates in 10% (w/v) RIPA buffer (0.5% Nonidet P-40, 0.5% sodium deoxycholate, 0.1% SDS, 10 mmol/l EDTA, and protease inhibitors). After 40 min of incubation in ice, samples were sonicated and cleared by centrifugation at 14,000 *x g* at 4 °C for 20 min. Supernatants were used for ROS and glutathione determinations and for immunoblotting.

Reactive Oxygen Species (ROS). ROS were measured using the 2',7'-dichlorofluorescein diacetate (DCFH-DA) probe. DCFH-DA is a stable, non-fluorescent molecule, that is hydrolyzed by esterases to non-fluorescent 2',7'-dichlorofluorescein (DCFH), which is rapidly oxidized in the presence of peroxides to the highly fluorescent 2',7'-dichlorofluorescein (DCF). Protein extracts were incubated with 5 μM of DCFH-DA for 15 min at 37° C, and then DCF was measured fluorimetrically at 485 nm excitation and 538 nm emission.

Oxidized-to-reduced glutathione ratio (GSSG/GSH). GSSG/GSH was assessed by mixing in a cuvette 0.05 M Na-phosphate buffer (pH 7.0), 1 mM EDTA (pH 7.0), and 10 mM dithionitrobenzoic acid (Sigma-Aldrich, St Louis, MO) plus an aliquot of the sample. After 2 min of reaction, GSH content was evaluated by reading absorbance at 412 nm, calculated referring to a standard curve, and expressed as μg/mg protein. Suitable volumes of diluted glutathione reductase and of reduced nicotinamide adenine dinucleotide phosphate were then added to convert the oxidized glutathione to the reduced form and then evaluate the total glutathione level. The difference between total glutathione and GSH content represents the GSSG content, also expressed as μg/mg protein.

Immunoblotting. SDS-PAGE was performed on 12% acrylamide (Sigma-Aldrich, St Louis, MO, USA) gel, loading 30 μg protein/well. Separated proteins were electro-transferred onto PVDF membrane (BioRad Laboratories, Inc.) and probed with anti- Manganese Superoxide Dismutase (Mn-SOD) antibody (1:1500 dilution, Upstate, Millipore, USA) and with anti α-tubulin antibody (1:100 dilution, Abcam, UK) to check protein loading. Proteins were detected with Pierce Super Signal chemiluminescent substrate following the manufacturer's instructions. Bands were photographed and analyzed using Image J software.

Statistical analysis. Data are expressed throughout the text as means ± SD, calculated from at least three different experiments. Comparison between groups was performed with analysis of variance (one-way ANOVA) and the threshold of significance was calculated with the Bonferroni test. Statistical significance was set at $p<0.05$.

Results

Physico-chemical characteristics of nanobubble formulation

Doxorubicin-loaded NBs showed an average diameter of about 350 nm and positive surface charge (Table 1). A prolonged drug release kinetics of doxorubicin from doxorubicin-loaded nanobubbles was demonstrated in *in vitro* release studies, as previously reported (Marano et al., 2016).

In particular, less than 10% of the drug was released from nanobubbles and no initial burst effect was observed, after 6 hours in the absence of ESW. On the contrary, following ESW treatment doxorubicin was released in a larger extent from nanobubbles.

Anti-tumor effects. In order to establish the time needed to deliver NBs to the tumor, doxorubicin content was measured in tumors of ATC-bearing mice at different times after doxorubicin-loaded NB injection. As shown in Fig. 1A, after 30 minutes, the drug was already present in the tumor tissue, and no significant difference in drug content was observed up to 24 hours. Therefore, 1.5 hours was chosen as waiting time before ESW treatment, since this time better fitted with our ESW treatment schedule.

To test the anti-tumor effect of different treatments, ATC-bearing mice were randomly divided into three groups: control mice (CTRL), doxorubicin-treated mice (DOXO) and mice treated with doxorubicin-loaded NBs (NBs-DOXO). After 1.5 hours, one of the two tumors of each animal was treated with ESWs (0.59 mJ/mm^2, 500 pulses) and treatments were repeated once a week for a 21-day period. Treatments are schematized in Fig. 1B.

As shown in Fig. 1C, after 21 days, tumor volume was significantly reduced in mice that received the combined treatment with NBs-DOXO and ESWs with respect to CTRL ($p<0.01$), DOXO ($p<0.05$) and NBs-DOXO ($p<0.05$) groups. The significant increase of the tumor doubling time (Table 3) after the combined treatment (*vs* CTRL, $p<0.001$; *vs* DOXO, $p<0.001$; *vs* NBs-DOXO, $p<0.01$) was in agreement with the significant decrease of tumor volume. The most efficient anti-tumor effect of the combined treatment was already evident by visual observation of tumors at

sacrifice (Fig. 1D). Moreover, the combined treatment determined the greatest reduction in tumor weights (*vs* CTRL, DOXO, and NBs-DOXO, $p<0.001$) as demonstrated in Fig. 1E.

In accordance with these observations, at sacrifice, the highest doxorubicin content (Fig. 1F) was found in tumors treated with doxorubicin-loaded NBs plus ESWs (*vs* DOXO, $p<0.001$; *vs* NBs-DOXO, $p<0.001$).

To explore the mechanisms underlying the tumor growth inhibition, we evaluated apoptotic (Fig. 2A and 2B) and proliferating cells (Fig. 2C and 2D). As shown in Fig. 2B, the number of apoptotic cells in tumors treated with NBs-DOXO was significantly increased with respect to CTRL ($p<0.001$) and to DOXO ($p<0.01$) groups. But, was the combined treatment with NBs-DOXO and ESWs to determine the greatest number of apoptotic cells (*vs* CTRL, $p<0.001$; *vs* DOXO, $p<0.001$; *vs* NBs-DOXO, $p<0.01$).

Moreover, the combined treatment with NBs-DOXO and ESWs decreased PCNA positive cells with respect to any other condition (Fig. 2C). Fig. 2D shows the percentage of PCNA positive cells. In tumors treated with NBs-DOXO the percentage was significantly reduced with respect to CTRL ($p<0.001$) and to DOXO ($p<0.01$) groups. The combined treatment elicited the greatest reduction in the percentage of proliferating cells (*vs* CTRL, $p<0.001$; *vs* DOXO, $p<0.001$; vs NBs-DOXO, $p<0.01$).

Cardiotoxicity. At sacrifice, hearts of doxorubicin-treated mice showed areas of disorganized muscle fibres with poor cellularity (Fig. 3A). On the contrary, cardiac tissue of mice treated with NBs-DOXO conserved the same appearance of hearts of the CTRL group (Fig. 3A).

As collagen is usually found in fibrotic tissues (Hinz 2007), Masson's trichrome specific stain was performed. Extended collagen blue areas were observable in hearts of DOXO group, while they were present in a very little extension in CTRL and in NBs-DOXO groups (Fig. 3B). Indeed, the percentage of collagen areas in heart of DOXO group was significantly increased as compared to CTRL group ($p<0.001$, Fig. 3C). On the contrary, the percentage of collagen in hearts of NBs-

DOXO group was significantly reduced with respect to DOXO group ($p<0.001$, Fig. 3C) and was comparable to that of the CTRL group.

Moreover, doxorubicin significantly increased the expression of collagen type 1 alpha 1 (*Col1a1*; $p<0.05$, Fig. 3D,), and of alpha-smooth muscle actin (*α-sma*; $p<0.001$, Fig. 3E) genes, well established markers of cardiac fibrosis (Hinz 2007). Encapsulating the drug into NBs counteracted these increases and resulted in *Col1a1* and *α-sma* expression levels similar to those of the CTRL group ($p<0.05$ for *Col1a1*, Fig. 3D; $p<0.001$ for *α-sma*, Fig. 3E).

Being an index of doxorubicin-induced heart damage (Singal *et al.* 2000, Spallarossa *et al.* 2006, Mukhopadhyay *et al.* 2009, Zhao *et al.* 2010), oxidative stress was also assessed. Doxorubicin significantly induced cardiac ROS production (*vs* CTRL, $p<0.001$, Fig. 4A), increased GSSG/GSH ratio (*vs* CTRL, $p<0.01$, Fig. 4B) and Mn-SOD protein expression (*vs* CTRL, $p<0.05$, Fig. 4C and D). Notably, in hearts of NBs-DOXO treated mice, ROS levels, GSSG/GSH ratio and Mn-SOD were significantly reduced with respect to DOXO group ($p<0.001$, Fig. 4A; $p<0.05$, Fig. 4B; $p<0.05$, Fig. 4C and D), and comparable to those of the CTRL group. In accordance with these observations doxorubicin was detected only in hearts of DOXO group whereas it was undetectable in hearts of NBs-DOXO group (Fig. 4E).

Discussion

The present *in vivo* preclinical study demonstrates that in ATC, a lethal tumor with no standard therapy, the combined treatment with doxorubicin-loaded glycol chitosan NBs and ESWs enhances the anti-tumor effects of doxorubicin and, at the same time, prevents the drug-induced heart damage.

Doxorubicin delivery to the tumor cells, with the specific aim to increase its anti-tumor efficacy and to reduce its side effects, is an important goal in ATC therapy. In fact, even if doxorubicin is the only chemotherapeutic drug approved for ATC treatment in monotherapy (Haddad *et al.* 2015), it has a poor clinical response (Giuffrida and Gharib 2000), and it causes severe dose-dependent side effects among which cardiotoxicity is the most prominent (Minotti *et al.* 2004, Chatterjee *et al.* 2010, Zhang *et al.* 2012).

Based on the promising results of our recent *in vitro* study (Marano *et al.* 2016), where we delineated the cytotoxic effects and the mechanism of this new combined treatment with NBs-DOXO and ESWs, we here go further moving to a xenograft *in vivo* model. Even if the cytotoxic efficacy of different types of nanoparticles to deliver doxorubicin has been reported in other tumor histotypes (Du *et al.* 2011, Wohlfart *et al.* 2011, Barenholz 2012, Golla *et al.* 2013, Yu *et al.* 2014, Fan *et al.* 2016, Lin *et al.* 2016, Razavi-Azarkhiavi *et al.* 2016); to date, no other study has used delivery systems to target doxorubicin in ATC. In 2011 Du et al. showed that US-responsive doxorubicin-loaded PEGylated perfluoropentane NBs resulted in a more efficient inhibition of tumor growth in hepatocarcinoma-bearing mice (Du *et al.* 2011). Others reported a greater anti-tumor efficacy in human prostate cancer xenograft model using doxorubicin-loaded lipid NBs in combination with US (Fan *et al.* 2016). In nude mice xenograft of fibrosarcoma, the combination of US with asparagine–glycine–arginine (NGR) peptide modified NBs, loaded with doxorubicin conjugated with cell-permeable peptides, resulted in higher tumor growth inhibition with respect to NBs or doxorubicin alone (Lin *et al.* 2016).

In 2012, Cavalli *et al.* developed stable chitosan NBs able to release DNA into COS7 cells after US treatment. In the presence of US, the perfluoropentane of the nanobubble core, which is liquid at room temperature, underwent a conversion from droplet to bubble at 37°C, inducing DNA release into the cells (Cavalli *et al.* 2012). The US-responsive doxorubicin-loaded nanoparticulate system prepared in 2011 by Du *et al.* was based on the same mechanism (nanodroplet/NB transition). Indeed, PEGylated perfluoropentane nanodroplets were converted into NBs at 37° C and only little drug was released if no US was applied (Du *et al.* 2011).

The novelty of both our previous (Marano *et al.* 2016) and present works is not only the use of new perfluoropentane drug-loaded NBs, but it is especially the use of ESWs as novel physical strategy to trigger drug release from NBs, specifically at the tumor site. Indeed, unlike US, ESWs have not heating effects and this characteristic could be an advantage for *in vivo* applications, since temperature increase is difficult to control spatially and temporally, especially in large tumors with heterogeneous vascularization, such as ATC (Diederich and Hynynen 1999).

In our xenograft murine model of human ATC, after doxorubicin-loaded NB injection in the tail vein, the drug was already detected in tumors after 30 minutes, accordingly to the above studies where a 30-minute waiting time before US treatment has been reported (Du *et al.* 2011, Fan *et al.* 2016, Lin *et al.* 2016). As in our experimental conditions the drug concentration remained stable up to 24 hours, we chose a 1.5 hour lag time before applying ESWs, since this time better fitted with our ESW treatment schedule. At the end of the 21-day period, combining doxorubicin-loaded NBs and ESWs elicited the best effect in term of tumor growth inhibition, reducing tumor volumes and weights and extending the tumor doubling time. The greatest doxorubicin accumulation observed in tumors treated with drug-loaded NBs plus ESWs paralleled the anti-tumor effect. Present data further confirm our previous *in vitro* results, where the combination of ESWs with doxorubicin-loaded NBs elicited the greatest intracellular drug accumulation in ATC cells, and significantly

increased doxorubicin cytotoxicity decreasing the drug Growth Inhibition Fifty of about 40 % (Marano *et al.* 2016).

Furthermore, we here demonstrated that loading doxorubicin into NBs avoided doxorubicin-induced heart damage and oxidative stress. In fact, whereas doxorubicin induced disorganization of muscle fibers, hearts of mice treated with doxorubicin-loaded NBs had a normal morphological aspect. Moreover, loading doxorubicin into NBs, prevented the increase of the fibrosis markers *Col1a1* and *α-sma*, determined by free doxorubicin. Doxorubicin is a conventional anthracycline acting by intercalation with DNA base pairs (Minotti *et al.* 2004) or through inhibition of topoisomerase I and II by direct linking to the two enzymes (Tacar *et al.* 2013). ROS production is another mechanism of doxorubicin anti-tumor activity that causes direct damage to the DNA, RNA, lipids and proteins (Sinha *et al.* 1987). However, doxorubicin-induced cardiomyopathy is strongly linked to an increase in cardiac oxidative stress and the induction of free radical production is the main mechanism through which doxorubicin injures the myocardium (Singal *et al.* 2000, Spallarossa *et al.* 2006, Mukhopadhyay *et al.* 2009, Zhao *et al.* 2010). Loading doxorubicin into NBs determined inhibition of doxorubicin-induced ROS production, and reduction of both GSSG/GSH ratio and Mn-SOD protein. ROS have an important role in the progression of fibrosis modulating fibroblast proliferation and differentiation into myofibroblasts expressing α-SMA and producing extracellular matrix proteins, as type 1 collagen (Krstić *et al.* 2015, Kuwahara *et al.* 2002). The absence of the drug in hearts of mice treated with doxorubicin-loaded NBs explained the prevention of cardiac side effects. As the probability of developing cardiomyopathy is largely dose-dependent (Sheppard *et al.* 2013), the possibility to use lower drug doses, together with delivering doxorubicin to the tumor tissue, is fundamental to reduce drug accumulation in not-target districts.

Summarizing, the drug delivery system presented in this study, by adding ESWs as physical trigger to glycol chitosan doxorubicin-loaded NBs, allowed increasing drug content in tumor tissue favoring the increase of doxorubicin anti-tumor effect with respect to the classic treatment with the

free drug. Moreover, the use of glycol chitosan NBs, reduced doxorubicin accumulation in heart avoiding cardiac oxidative stress and fibrosis.

In conclusion, this preclinical study on the use of ESWs and doxorubicin-loaded NBs suggests that this combined treatment may be a promising drug delivery tool for precisely targeting doxorubicin to ATC. The possibility to focus ESWs with high precision in depth without heating effect, with consequent controlled drug release in the tumor tissue, makes this new strategy feasible for other aggressive solid tumors in which chemotherapy unfortunately remains the first option.

Given these promising results and the lack of a standard therapy for ATC, the further step will be clinical trials with the hope to open new perspectives for improving ATC treatment and patient quality of life.

Declaration of interest: The authors declare no potential conflicts of interest.

Funding: Fondazione CRT (grant number= RF2013.1289), Turin, Italy to MGC. "Research Fund ex-60%", University of Turin, Turin, Italy to MGC and to RC.

Acknowledgments

We thank Massimo Cedrino, Federica Antico and Alessia Cento for technical support.

References

Azzi S, Hebda JK, Gavard J 2013 Vascular permeability and drug delivery in cancers. *Frontiers in oncology* **3** 211.

Barenholz YC 2012 Doxil®--the first FDA-approved nano-drug: lessons learned. *Journal of controlled release* **160** 117-134.

Canaparo R, Serpe L, Zara GP, Chiarle R, Berta L, Frairia R 2008 High energy shock waves (ESW) increase paclitaxel efficacy in a syngeneic model of breast cancer. *Technology in cancer research & treatment* **7** 117-124.

Carmeliet P, Jain RK 2011 Principles and mechanisms of vessel normalization for cancer and other angiogenic diseases. *Nature reviews. Drug discovery* **10** 417-427.

Catalano MG, Costantino L, Fortunati N, Bosco O, Pugliese M, Boccuzzi G, Berta L, Frairia R 2007 High energy shock waves activate 5'-aminolevulinic Acid and increase permeability to Paclitaxel: antitumor effects of a new combined treatment on anaplastic thyroid cancer cells. *Thyroid* **17** 91-99.

Cavalli R, Bisazza A, Trotta M, Argenziano M, Civra A, Donalisio M, Lembo D 2012 New chitosan nanobubbles for ultrasound-mediated gene delivery: preparation and in vitro characterization. *International journal of nanomedicine* **7** 3309-3318.

Cavalli R, Soster M, Argenziano M 2016 Nanobubbles: a promising efficient tool for therapeutic delivery. *Therapeutic delivery* **7** 117-138.

Chatterjee K, Zhang J, Honbo N, Karliner JS 2010 Doxorubicin cardiomyopathy. *Cardiology* **115** 155-162.

Collis J, Manasseh R, Liovic P, Tho P, Ooi A, Petkovic-Duran K, Zhu Y 2010 Cavitation microstreaming and stress fields created by microbubbles. *Ultrasonics* **50** 273-279.

Diederich CJ, Hynynen K 1999 Ultrasound technology for hyperthermia. *Ultrasound in medicine & biology* **25** 871-887.

Du L, Jin Y, Zhou W, Zhao J 2011 Ultrasound-triggered drug release and enhanced anticancer effect of doxorubicin-loaded poly(D,L-lactide-co-glycolide)-methoxy-poly(ethylene glycol) nanodroplets. *Ultrasound in medicine & biology* **37** 1252-1258.

Fan X, Wang L, Guo Y, Xiong X, Zhu L, Fang K 2016 Inhibition of prostate cancer growth using doxorubicin assisted by ultrasound-targeted nanobubble destruction. *International journal of nanomedicine* **11** 3585-3596.

Fang J, Nakamura H, Maeda H 2011 The EPR effect: Unique features of tumor blood vessels for drug delivery, factors involved, and limitations and augmentation of the effect. *Advanced drug delivery reviews* **63** 136-151.

Frairia R, Catalano MG, Fortunati N, Fazzari A, Raineri M, Berta L 2003 High energy shock waves (HESW) enhance paclitaxel cytotoxicity in MCF-7 cells. *Breast cancer research and treatment* **81** 11-19.

Gao Z, Kennedy AM, Christensen DA, Rapoport NY **2008** Drug-Loaded Nano/Microbubbles for Combining Ultrasonography and Targeted Chemotherapy *Ultrasonics* **48** 260-270.

Giuffrida D, Gharib H 2000 Anaplastic thyroid carcinoma: current diagnosis and treatment. *Annals of oncology* **11** 1083-1089.

Golla K, Bhaskar C, Ahmed F, Kondapi AK 2013 A target-specific oral formulation of Doxorubicin-protein nanoparticles: efficacy and safety in hepatocellular cancer. *Journal of Cancer* **4** 644-652.

Guo DD, Xu CX, Quan JS, Song CK, Jin H, Kim DD, Choi YJ, Cho MH, Cho CS 2009 Synergistic anti-tumor activity of paclitaxel-incorporated conjugated linoleic acid-coupled poloxamer thermosensitive hydrogel in vitro and in vivo. *Biomaterials* **30** 4777-4785.

Haddad RI, Lydiatt WM, Ball DW, Busaidy NL, Byrd D, Callender G, Dickson P, Duh QY, Ehya H, Haymart M *et al.* 2015 Anaplastic Thyroid Carcinoma, Version 2.2015. *J Journal of the National Comprehensive Cancer Network* **13** 1140-1150.

Hinz B 2007 Formation and function of the myofibroblast during tissue repair. *The Journal of investigative dermatology* **127** 526-537.

Kodama T, Doukas AG, Hamblin MR 2002 Shock wave-mediated molecular delivery into cells. *Biochimica et biophysica acta* **1542** 186-194.

Krstić J, Trivanović D, Mojsilović S, Santibanez JF 2015 Transforming growth factor-beta and oxidative stress interplay: implications in tumorigenesis and cancer progression. *Oxidative medicine and cellular longevity* **2015** 654594.

Kuwahara F, Kai H, Tokuda K, Kai M, Takeshita A, Egashira K, Imaizumi T 2002 Transforming growth factor-beta function blocking prevents myocardial fibrosis and diastolic dysfunction in pressure overloaded rats. *Circulation* **106** 130-135.

Lauer U, Bürgelt E, Squire Z, Messmer K, Hofschneider PH, Gregor M, Delius M 1997 Shock wave permeabilization as a new gene transfer method. *Gene therapy* **4** 710-715.

Lin W, Xie X, Deng J, Liu H, Chen Y, Fu X, Liu H, Yang Y 2016 Cell-penetrating peptide-doxorubicin conjugate loaded NGR-modified nanobubbles for ultrasound triggered drug delivery. *Journal of drug targeting* **24** 134-146.

Marano F, Argenziano M, Frairia R, Adamini A, Bosco O, Rinella L, Fortunati N, Cavalli R, Catalano MG 2016 Doxorubicin-loaded nanobubbles combined with extracorporeal shock waves: basis for a new drug delivery tool in anaplastic thyroid cancer. *Thyroid* **26** 705-716.

Minotti G, Menna P, Salvatorelli E, Cairo G, Gianni L 2004 Anthracyclines: molecular advances and pharmacologic developments in antitumor activity and cardiotoxicity. *Pharmacological reviews* **56** 185-229.

Mukhopadhyay P, Rajesh M, Bátkai S, Kashiwaya Y, Haskó G, Liaudet L, Szabó C, Pacher P 2009 Role of superoxide, nitric oxide, and peroxynitrite in doxorubicin-induced cell death in vivo and in vitro. *American journal of physiology. Heart and circulatory physiology* **296** H1466-H1483.

Palmero A, Berger M, Venturi C, Ferrero I, Rustichelli D, Berta L, Frairia R, Madon E, Fagioli F 2006 High energy shock waves enhance the cytotoxic effect of doxorubicin and methotrexate to human osteosarcoma cell lines. *Oncology reports* **15** 267-273.

Rassweiler JJ, Knoll T, Köhrmann KU, McAteer JA, Lingeman JE, Cleveland RO, Bailey MR, Chaussy C 2011 Shock wave technology and application: an update. *European urology* **59** 784-796.

Razavi-Azarkhiavi K, Jafarian AH, Abnous K, Razavi BM, Shirani K, Zeinali M, Jaafari MR, Karimi G 2016 The Comparison of Biodistribution, Efficacy and Toxicity of Two PEGylated Liposomal Doxorubicin Formulations in Mice Bearing C-26 Colon Carcinoma: a Preclinical Study. *Drug research* **66** 330-336.

Schweppe RE, Klopper JP, Korch C, Pugazhenthi U, Benezra M, Knauf JA, Fagin JA, Marlow LA, Copland JA, Smallridge RC *et al.* 2008 Deoxyribonucleic acid profiling analysis of 40 human thyroid cancer cell lines reveals cross-contamination resulting in cell line redundancy and misidentification. *The Journal of clinical endocrinology and metabolism* **93** 4331-4441.

Sheppard RJ, Berger J, Sebag IA 2013 Cardiotoxicity of cancer therapeutics: current issues in screening, prevention, and therapy. *Frontiers in pharmacology* **4** 19.

Singal PK, Li T, Kumar D, Danelisen I, Iliskovic N 2000 Adriamycin-induced heart failure: mechanism and modulation. *Molecular and cellular biochemistry* **20** 77-86.

Sinha BK, Katki AG, Batist G, Cowan KH, Myers CE 1987 Adriamycin-stimulated hydroxyl radical formation in human breast tumor cells. *Biochemical pharmacology* **36** 793-796.

Smallridge RC, Ain KB, Asa SL, Bible KC, Brierley JD, Burman KD, Kebebew E, Lee NY, Nikiforov YE, Rosenthal MS *et al.* 2012 American Thyroid Association guidelines for management of patients with anaplastic thyroid cancer. *Thyroid* **22** 1104-1039.

Smallridge RC, Copland JA 2010 Anaplastic thyroid carcinoma: pathogenesis and emerging therapies. *Journal of clinical oncology* **22** 486-497.

Spallarossa P, Altieri P, Garibaldi S, Ghigliotti G, Barisione C, Manca V, Fabbi P, Ballestrero A, Brunelli C, Barsotti A **2006** Matrix metalloproteinase-2 and -9 are induced differently by doxorubicin in H9c2 cells: the role of MAP kinases and NAD(P)H oxidase. *Cardiovascular research* **69** 736-745.

Tacar O, Sriamornsak P, Dass CR 2013 Doxorubicin: an update on anticancer molecular action, toxicity and novel drug delivery systems. *The Journal of pharmacy and pharmacology* **65** 157-170.

Wang CJ 2012 Extracorporeal shockwave therapy in musculoskeletal disorders. *Journal of orthopaedic surgery and research* **7** 11.

Wohlfart S, Khalansky AS, Gelperina S, Maksimenko O, Bernreuther C, Glatzel M, Kreuter J 2011 Efficient chemotherapy of rat glioblastoma using doxorubicin-loaded PLGA nanoparticles with different stabilizers. *PLoS One* **6** e19121.

Yu Y, Chen CK, Law WC, Weinheimer E, Sengupta S, Prasad PN, Cheng C 2014 Polylactide-graft-doxorubicin nanoparticles with precisely controlled drug loading for pH-triggered drug delivery. *Biomacromolecule* **15** 524-532.

Zhang S, Liu X, Bawa-Khalfe T, Lu LS, Lyu YL, Liu LF, Yeh ET 2012 Identification of the molecular basis of doxorubicin-induced cardiotoxicity. *Nature medicine* **18** 1639-1642.

Zhao Y, McLaughlin D, Robinson E, Harvey AP, Hookham MB, Shah AM, McDermott BJ, Grieve DJ 2010 Nox2 NADPH oxidase promotes pathologic cardiac remodeling associated with doxorubicin chemotherapy. *Cancer research* **70** 9287-9297.

Figures legends

Figure 1. Tumor growth inhibition. (A) Doxorubicin content at 0.5, 1.5, 5 and 24 hours after i.v. injection of doxorubicin-loaded NBs (n=5 per group) expressed as ng of drug/g tissue. (**B)** Schematic representation of the treatments of ATC-bearing mice. Two tumors per mouse were allowed to grow in the flanks of 7-week-old female NSG mice. When tumors reached an appropriate volume (100 mm^3), 100 μl vehicle, or 0.75 mg/kg doxorubicin solution, or 0.75 mg/kg doxorubicin-loaded NBs were i.v. injected into the tail vein. After 1.5 hours, one tumor for each mouse was treated with ESWs. (**C)** Tumor volumes at 0, 7, 14 and 21 days (n=5 per group), calculated with the formula a^2 x b x 0.5, where a is the shortest diameter and b is the diameter perpendicular to a. (**D)** Representative pictures of tumors after 21 days of treatment. **E)** Weights of tumors at 21 days (n=5 per group). (**F)** Doxorubicin content (n=5 per group) after 21 days of treatments expressed as ng of drug/g tissue.

Significances were calculated with one-way ANOVA analysis and Bonferroni post-test. Significance *vs* CTRL: p<0.05 (*); p<0.01 (**); p<0.001 (***). Significance *vs* DOXO: p<0.05 (#); p<0.01 (##); p<0.001 (###). Significance plus ESWs *vs* no ESWs: p<0.05 (°); p<0.01 (°°); p<0.001 (°°°).

Figure 2. Apoptosis and proliferation of tumor cells. (**A)** Representative pictures of TUNEL stained slides after 21 days of treatments (scale bar: 50 μm). (**B)** Quantification of apoptotic cells per field, excluding necrosis areas, by ImageJ software in 10 randomly chosen sections at x200 final magnification (n=5 per group). (**C)** Representative pictures of PCNA slides after 21 days of treatments (scale bar: 50 μm). (**D)** Percentage of PCNA positive cells per field quantified by ImageJ software counting 10 randomly chosen x200 final magnification (n=5 per group).

Significances were calculated with one-way ANOVA analysis and Bonferroni post-test. Significance *vs* CTRL, p<0.001 (***); significance *vs* DOXO, p<0.01 (##), p<0.001 (###); significance plus ESWs *vs* no ESWs, p<0.01 (°°).

Figure 3. Heart fibrosis. (**A)** Representative pictures of Hematoxylin-Eosin stained heart slide scans (scale bar: 100 μm; n=5 per group). (**B)** Representative pictures of Masson's trichrome stained heart slides for collagen identification (scale bar: 50 μm; n=5 per group). (**C)** Percentage of blue area, corresponding to collagen fibers, *vs* total area counted on ten randomly chosen fields at x200 magnification by ImageJ software. (**D)** Cardiac gene expression of *col1a1* and (**E)** *α-sma* evaluated by RT-PCR (n=5 per group). Results are normalized *vs* three different housekeeping genes (ribosomal protein L13A, ribosomal protein large P0, and glyceraldehyde-3-phosphate dehydrogenase) and expressed as relative fold expression *vs* the CTRL group.

Significances were calculated with one-way ANOVA analysis and Bonferroni post-test. Significance *vs* CTRL, $p<0.05$ (*), $p<0.001$ (***); significance *vs* DOXO, $p<0.05$ (#), $p<0.001$ (###).

Figure 4. Oxidative stress in cardiac tissue. (**A)** ROS measured in heart tissue after 21 days of treatments (n=5 per group). Results were expressed as pmol/mg protein content. (**B)** GSSG and GSH content in cardiac tissue after 21 days of treatments (n=5 per group) expressed as ratio between GSSG and GSH content. (**C)** A typical Mn-SOD western blot on heart extracts is reported. (**D)** Western blot quantification by ImageJ software (n=5 per group). (**E)** Doxorubicin content in hearts after 21 days of treatments (n=5 per group) expressed as ng/g tissue.

Significances were calculated with one-way ANOVA analysis and Bonferroni post-test. Significance *vs* CTRL, $p<0.05$ (*), $p<0.01$ (**), $p<0.001$ (***); significance *vs* DOXO, $p<0.05$ (#), $p<0.001$ (###).

Table 1. **Physico-chemical characteristics of NB formulations.**

	Empty NBs	Doxorubicin-loaded NBs
Average diameters ± SD (nm)	**344.6 ± 13.8**	**356.2 ± 15.1**
PDI (Polydispersity Index)	**0.19 ± 0.01**	**0.20 ± 0.02**
ζ-Potential ± SD (mV)	**29.8 ± 2.122**	**30.4 ± 2.85**
Encapsulation efficiency	**-**	**75 %**
Loading capacity	**-**	**4.5 %**

Table 2. **Primers for Real-time PCR.**

GENE	PRIMERS
α- sma (alpha-smooth muscle actin)	Sense:5'-GCCAGTCGCTGTCAGGAACC-3' Antisense:5'-CAGAGCCCAGAGCCATTGTCG-3'
Col1 A1 (collagen type 1 alpha 1)	Sense:5'-GCCACTGCCCTCCTGACG-3' Antisense:5'-AGATCAAGCATACCTCGGGTTTCC-3'
L13A (ribosomal protein L13a)	Sense: 5'-GTGGTCCCTGCTGCTCTCAAG-3' Antisense: 5'-GCTGTCACTGCCTGGTACTTCC-3'
Rplp0 (ribosomal protein, large, P0)	Sense:5'-AGGAAGAGTCGGAGGAATCAGATG-3' Antisense:5'-CTTGGTTGCTTTGGCGGGATTAG-3'
Gapdh (glyceraldehyde-3-phosphate dehydrogenase)	Sense:5'-AGCAAGGACACTGAGCAAGAGAG-3' Antisense:5'-GGGATGGAAATTGTGAGGGAGATG-3'

Table 3. Doubling time[1] of tumor volume.

TREATMENT	DOUBLING TIME (DAYS)
CTRL	11.2 ± 0.4
ESWs	12.3 ± 1
DOXO	11.2 ± 0.2
DOXO + ESWs	14.8 ± 2.4
NBs-DOXO	14 ± 1.3
NBs-DOXO + ESWs	24.5 ± 4.3 (***)(###)(°°) [2]

[1] Doubling time of tumor volume was estimated according to the formula described by Guo and colleagues et al. (29) and reported in methods section.

[2]Significances were calculated with one-way ANOVA analysis and Bonferroni post-test. Significance *vs* CTRL: $p<0.001$ (***). Significance *vs* DOXO: $p<0.001$ (###). Significance plus ESWs *vs* no ESWs: $p<0.01$ (°°).

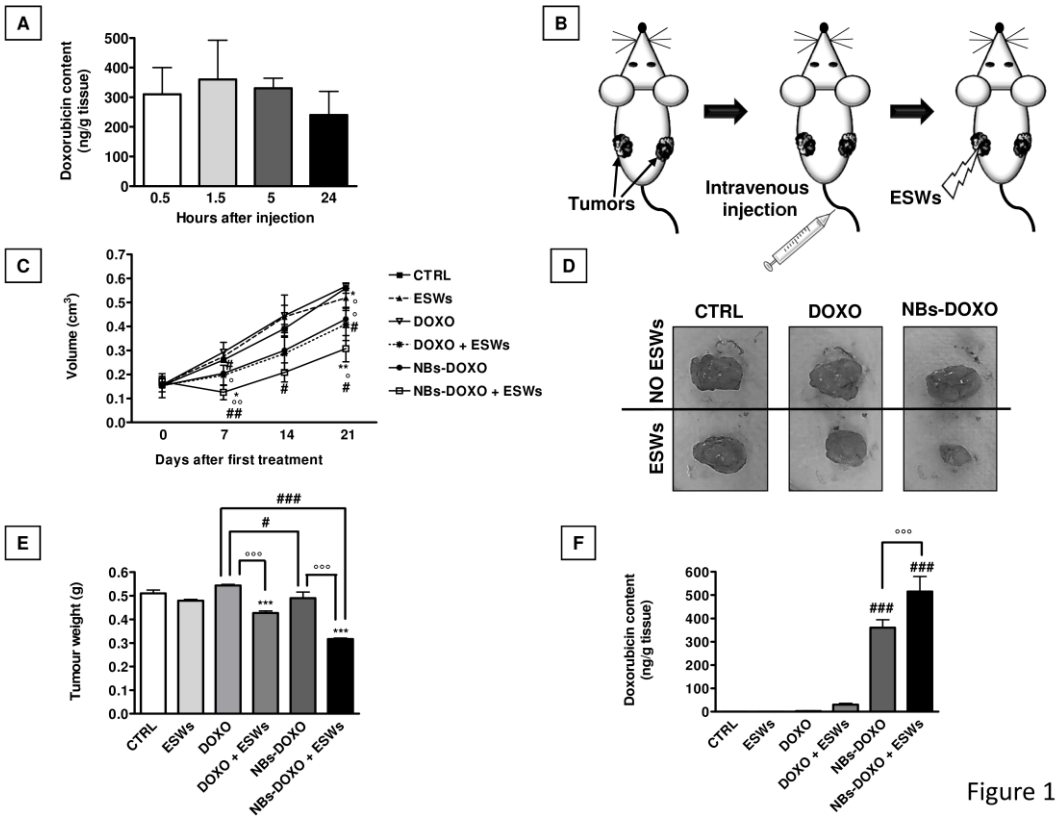

Figure 1

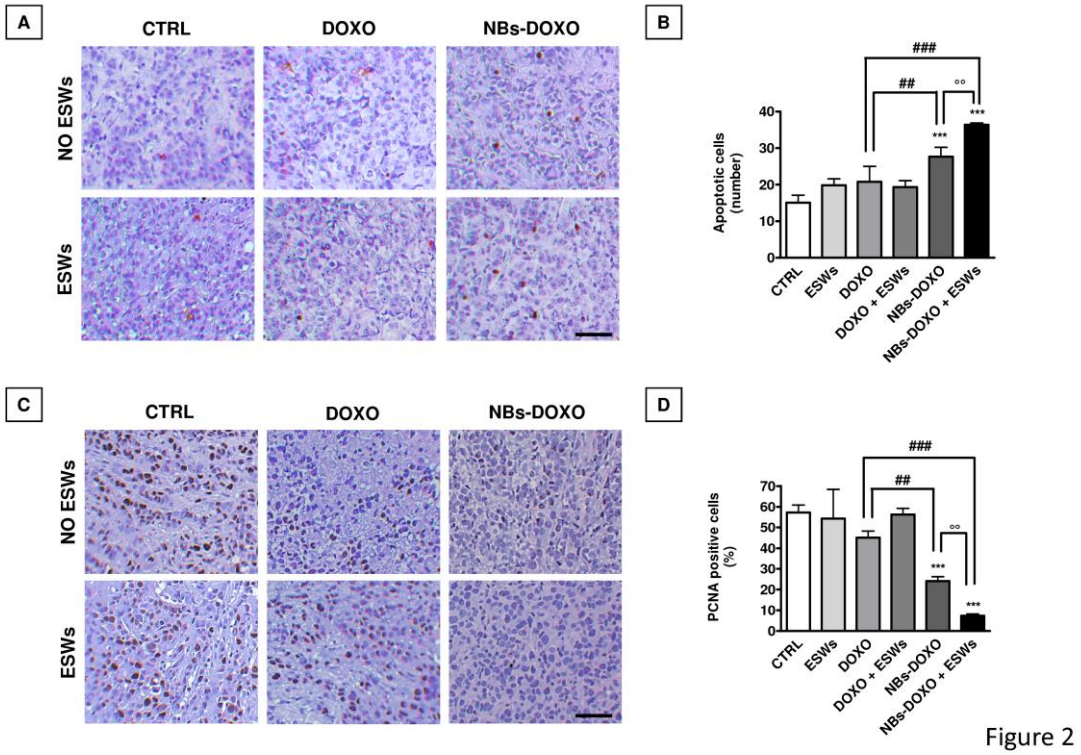

Figure 2

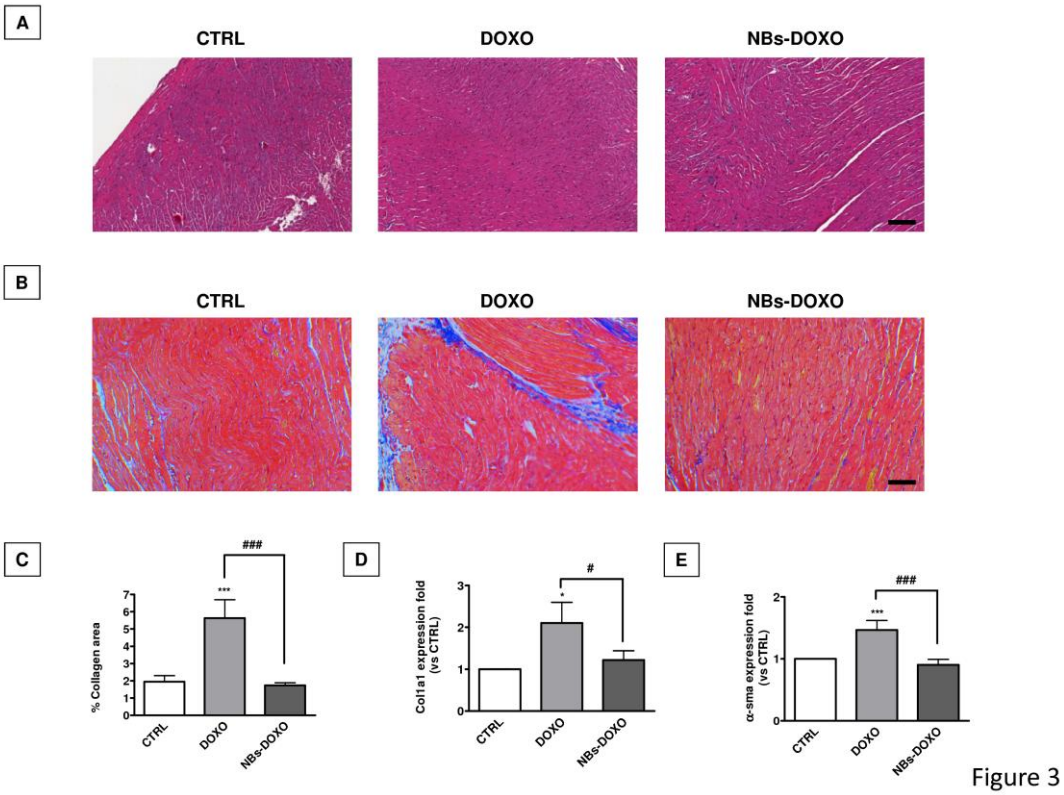

Figure 3

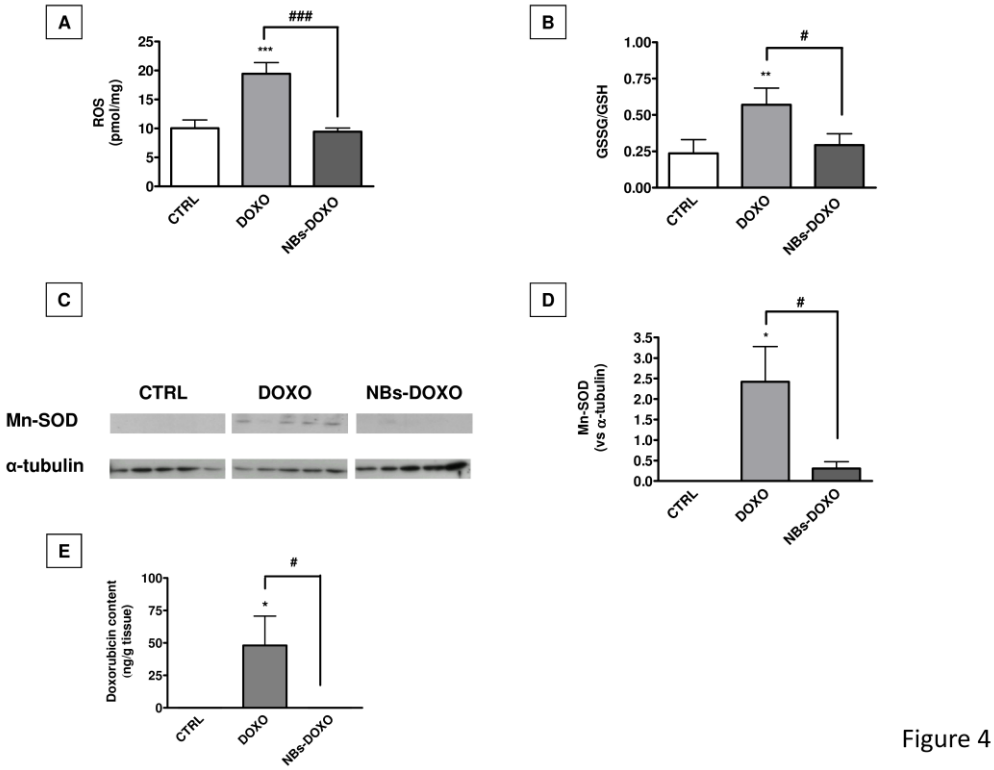

Figure 4